NANO LETTERS

pubs.acs.org/NanoLett

Letter

Superconducting Contacts to a Monolayer Semiconductor

Mehdi Ramezani, Ian Correa Sampaio, Kenji Watanabe, Takashi Taniguchi, Christian Schönenberger, and Andreas Baumgartner*

Cite This: *Nano Lett.* 2021, 21, 5614–5619

Read Online

ACCESS | Metrics & More | Article Recommendations | Supporting Information

ABSTRACT: We demonstrate superconducting vertical interconnect access (VIA) contacts to a monolayer of molybdenum disulfide (MoS_2), a layered semiconductor with highly relevant electronic and optical properties. As a contact material we use MoRe, a superconductor with a high critical magnetic field and high critical temperature. The electron transport is mostly dominated by a single superconductor/normal conductor junction with a clear superconductor gap. In addition, we find MoS_2 regions that are strongly coupled to the superconductor, resulting in resonant Andreev tunneling and junction-dependent gap characteristics, suggesting a superconducting proximity effect. Magnetoresistance measurements show that the bandstructure and the high intrinsic carrier mobility remain intact in the bulk of the MoS_2. This type of VIA contact is applicable to a large variety of layered materials and superconducting contacts, opening up a path to monolayer semiconductors as a platform for superconducting hybrid devices.

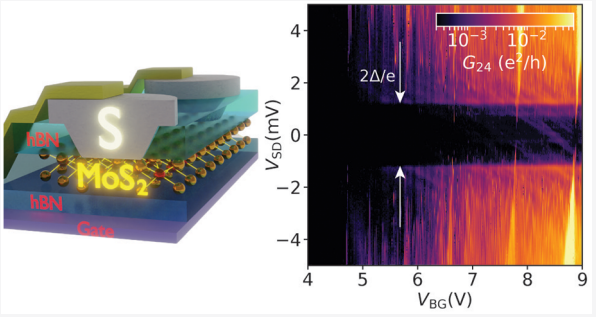

KEYWORDS: *TMDC, van der Waals heterostructure, MoS_2, monolayer semiconductor, superconducting contacts, superconducting proximity effect*

Semiconductors combined with superconducting metals have become a most fruitful field for applications and fundamental research, from gate tunable superconducting qubits[1] and thermoelectrics[2,3] to prospective Majorana bound states,[4,5] or sources of entangled electron pairs.[6−8] These experiments were mainly developed based on one-dimensional (1D) nanowires. To obtain more flexible platforms and scalable architectures, recent efforts focused on two-dimensional (2D) semiconductors.[9−13] However, the number of materials suitable for superconducting hybrids is rather limited. Potentially ideal and ultimately thin semiconductors with a large variety of properties can be found among transition metal dichalcogenides (TMDCs) grown in stacked atomically thin layers. TMDCs often exhibit a broad variety of interesting optical and electronic properties,[14−16] for example the valley degree of freedom, potentially useful as qubits,[17,18] strong electron−electron[19,20] and spin−orbit interactions,[20] or crystals with topologically nontrivial bandstructures.[21,22] One promising material is the semiconductor MoS_2 with a relatively high mobility and large mean free path, allowing for gate-defined nanostructures,[23−25] which would make MoS_2 an ideal platform to combine with superconducting elements.

MoS_2 was used as a tunnel barrier between superconductors in vertical heterostructures[26,27] and showed signs of intrinsic superconductivity[28] and of a ferromagnetic phase at low electron densities.[29] However, to exploit the intrinsic properties of MoS_2 and to fabricate in situ gate tunable superconducting hybrid structures, direct superconducting contacts in lateral devices are required. Such contacts are difficult to fabricate due to the formation of Schottky barriers,[21,30,31] material degradation,[32] and fabrication residues when using standard fabrication methods.[24,33,34] Less conventional edge contacts were also found problematic recently.[35]

Here, we report vertical access interconnect (VIA) contacts[36] to monolayer MoS_2 with the superconductor MoRe as contact material. We demonstrate a clear superconducting gap in the transport characteristics, including the magnetic field and temperature dependence, and features suggesting stronger superconductor−semiconductor couplings, forming the basis for superconducting proximity effects and bound states. In addition, we show that this fabrication method retains the intrinsic MoS_2 bulk properties, including a large electron mobility and sequentially occupied spin−orbit split bands.[23]

Figure 1a shows an optical microscopy image of the presented device, and a schematic of a single VIA contact. The MoS_2 is fully encapsulated by exfoliated hexagonal boron

Received: February 11, 2021
Revised: June 2, 2021
Published: June 23, 2021

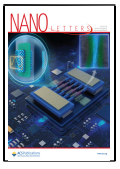

https://doi.org/10.1021/acs.nanolett.1c00615
Nano Lett. 2021, 21, 5614–5619

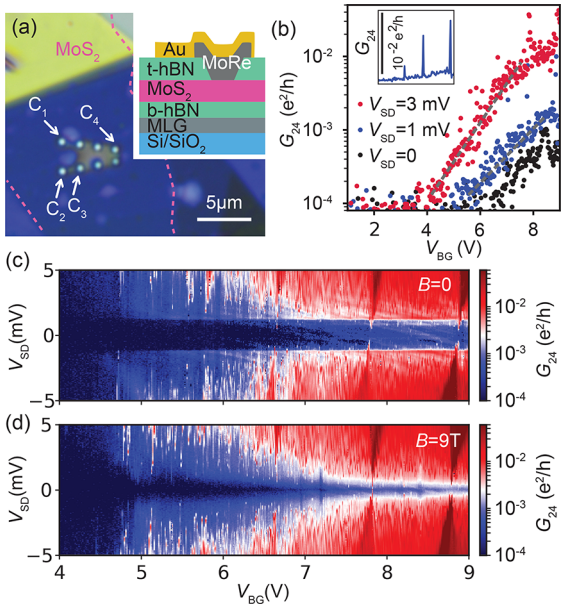

Figure 1. (a) Optical microscopy image of the MoS_2 heterostructure with MoRe VIA contacts pointed out by white arrows. Inset: schematic of a VIA contact with t-hBN and b-hBN denoting the top and bottom hBN layers, respectively. (b) Differential conductance G_{24} as a function of V_{BG} for a series of V_{SD} on a logarithmic scale and as an inset for V_{SD} = 1 mV on a linear scale. (c) G_{24} versus V_{BG} and V_{SD} at B = 0 and (d) at B = 9 T.

nitride (hBN), ensuring minimal contamination of the bulk materials, while the following assembly process allows the fabrication of pristine material interfaces and contacts, for example never directly exposing the active contact area to air:

(1) Vertical access: using electron beam lithography (EBL), VIA areas with a radius of 200 nm are defined on the designated top hBN flake (~40 nm thickness) on a Si/SiO_2 wafer, and etched completely open by reactive ion etching with a 20:5:5 sccm $SF_6/O_2/Ar$ mixture at 25 mTorr chamber pressure and 50 W RF power.

(2) VIA metalization: in a second EBL step, a slightly larger area with the VIA in the center is defined for mechanical anchoring to the top hBN. We then deposit the type II superconductor MoRe (bulk critical temperature $T_c \approx 6-10$ K, (second) critical magnetic field $B_c \approx 8-9$ T[37,38]) using sputter techniques. As the optimal film thickness we find 10 nm plus the top hBN thickness.

(3) Stacking of layers: the wafer with the VIA structure is transferred to an inert gas (nitrogen) glovebox (residual water and oxygen levels of <0.1 ppm), where the top hBN layer with the metalized VIAs is picked up from the substrate using a polycarbonate (PC) stamp and an hBN helper layer and then used to pick up consecutively a monolayer MoS_2 flake, a bottom hBN flake (~25 nm thickness), and a multilayer graphene (MLG) flake serving as backgate.

(4) Finish: the stack is then deposited onto a Si/SiO_2 wafer, where macroscopic Ti/Au (10/50 nm) leads to the VIAs are fabricated using EBL. The sample is then annealed at 350 °C for 30 min in a vacuum chamber with a constant flow of forming gas.

Using gold as VIA material, this fabrication process yields >80% of the contacts with two-terminal resistance-area products smaller than 200 kΩ μm^2 at T = 1.7 K at a backgate voltage of V_{BG} = 10 V. This yield is reduced to ~65% when using MoRe, possibly due to a material loss during the pick-up procedure. In the presented device, only half of the contacts show resistances lower than 200 kΩ μm^2, which we use for the experiments and are labeled from C_1 to C_4 in Figure 1a. The contacts were fabricated at various distances, stated individually for each discussed contact pair, all in the range of a few micrometers. The two terminal differential conductances $G_{jk} = dI_j/dV_k$ we obtain by measuring the current variation in the grounded contact C_j while applying a modulated bias voltage V_{SD} to contact C_k using standard lock-in techniques. The experiments were performed in a dilution refrigerator at ~60 mK, while for higher temperatures we used a variable temperature insert (VTI) with a base temperature of ~1.7 K. In addition, we apply an external magnetic field B perpendicular to the substrate.

In Figure 1b, the differential conductance G_{24} (center to center contact distance: 4.85 μm) is plotted as a function of the backgate voltage V_{BG} for several bias voltages V_{SD}. Increasing V_{BG} results in an exponential increase in G_{24}, starting from a pinch-off voltage of $V_{BG} \approx 6$ V for $V_{SD} = 0$. This value is offset toward smaller values for larger bias voltages, a first indication for an energy gap. However, as seen in the inset of Figure 1b, in this regime we find very sharp peaks in G, consistent with Coulomb blockade (CB) effects. We note that an increase in V_{BG} not only changes the charge carrier density in the MoS_2, but also the Schottky barrier at the metal–semiconductor interface and disorder induced charge islands. To demonstrate a superconducting energy gap and to distinguish it from other effects like CB, we plot in Figure 1c the conductance G_{24} versus V_{SD} over a large range of V_{BG} at B = 0, while Figure 1d shows the same experiment at B = 9 T. At B = 0, independent of the gate voltage, one clearly finds a strongly suppressed conductance for roughly $|V_{SD}| < 1.2$ mV, a gap size consistent with literature values for the superconducting energy gap of MoRe.[39] Similar data for a second device are shown in Supporting Information, Figure S1. The conductance is suppressed by a factor ~8 between the large and the zero bias values at $V_{BG} \approx 6$ V, and by a factor of ~15 near V_{BG} = 8 V. We note that such a sharp gap is only observable if a tunnel barrier is formed between the semiconducting MoS_2 and the superconducting region, at least at one contact. The discrete features inside the gap are probably not Andreev bound states,[40,41] but rather originate from gate-modulated conductance features in the bulk MoS_2. At $|V_{SD}| > 1.2$ mV, we find a strong modulation of G, which we interpret as several Coulomb blockaded regions. These resonances suggest that there is significant disorder near some of these contacts, so that we can think of this device as an MoS_2 region, incoherently coupled to the contacts by two normal-superconductor (N/S) junctions. The reason for one junction, namely the less transparent one, dominating the transport characteristics is that the junction with the higher transmission has a reduced resistance in the energy gap due to Andreev reflection, in which two electrons are transferred to S to form a Cooper pair. At B = 9 T, the superconducting gap is reduced, as discussed below in detail, but we now find that the gap becomes gate dependent. While in short semiconducting nanowires a gate tunable proximity effect was reported,[42,43] we tentatively attribute our finding to a gate independent superconducting energy gap convoluted with a gate tunable MoS_2 conductance.

We investigate the gap in the transport characteristics and the field dependence in more detail in Figure 2 for the same

https://doi.org/10.1021/acs.nanolett.1c00615
Nano Lett. 2021, 21, 5614–5619

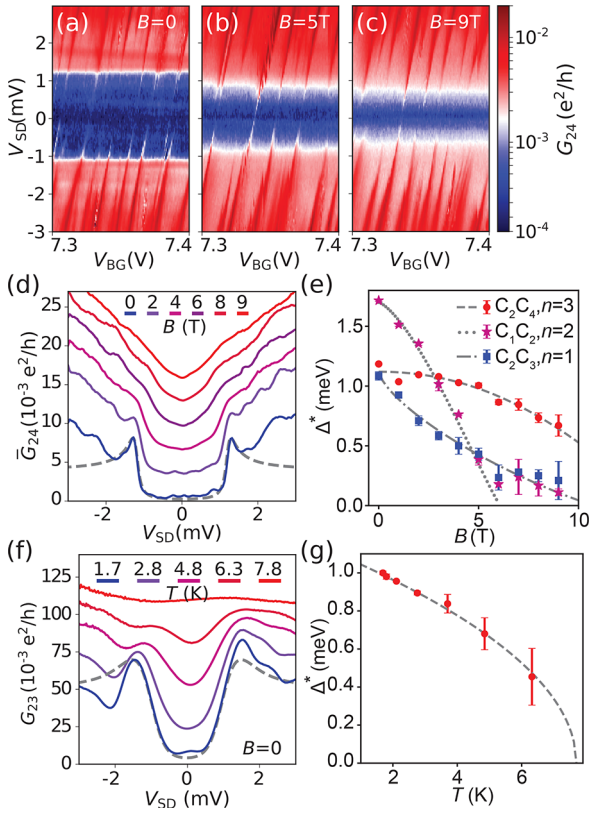

Figure 2. (a) Differential conductance G_{24} as a function of the bias V_{SD} and the backgate voltage V_{BG} at B = 0, (b) B = 5 T, and (c) B = 9 T. (d) G_{24} averaged over a V_{BG} interval of 0.5 V plotted versus V_{SD} for the indicated magnetic fields with the curves offset for clarity. (e) Superconducting energy gap Δ* as a function of B for different contact pairs. Δ* is extracted from the inflection points in the curves of Figure 2d [red disks], from Figure 3 [purple stars], and from an additional data set discussed in Supporting Information, Figure S2 [blue rectangles]. (f) G_{23} versus V_{SD} recorded at the indicated temperatures T. (g) Δ* versus T extracted from the data in (f). All theoretical curves (dashed and dotted lines) are discussed in the text.

contact pair. Similar data were found for the other contact pairs and on two more devices, with an additional example provided in Supporting Information, Figure S1. Figure 2a–c shows higher-resolution conductance maps for a smaller V_{BG} interval for the magnetic fields B = 0, B = 5 T, and B = 9 T, respectively. The figures show a very clear gap in the conductance map, which is systematically reduced with increasing magnetic field, independently of the sharp resonances. The positions of the latter are unaffected by the gap, so that we can attribute them to resonances in the MoS_2, for example due to CB. To extract the energy gap, we plot G_{24} in Figure 2d, averaged over a gate voltage interval of 0.5 V for each V_{SD} value, for a series of perpendicular magnetic fields. These curves show how the energy gap closes with increasing B. The curve at B = 0 can be fitted well using the model by Blonder, Tinkham, and Klapwjik (BTK),[44] including an additional broadening parameter,[45] as shown in Figure 2d by a gray dashed line. The fit parameters are consistent with a weakly transmitting barrier in a single N/S junction. At larger fields, the extracted parameters become ambiguous due to a strong broadening of the curves. As a measure for the superconducting energy gap Δ*, we therefore plot in Figure 2e the average of the low-bias inflection points of each curve (red dots). For B = 0, we find $\Delta_0^* \approx 1.2$ meV, in good agreement with bulk MoRe[26,39] and one S/N junction dominating the transport. The field dependence of Δ* is well described by standard theory of superconductivity for pair-breaking impurities in a metal with a mean free path shorter than the superconducting coherence lengths. For the corresponding self-consistency equations, we use $\Delta^*(\alpha) = \hat{\Delta}(\alpha)[1 - (\alpha/\hat{\Delta}(\alpha))^{2/3}]^{3/2}$ with $\Delta^*(\alpha)$ the energy gap in the excitation spectrum and $\hat{\Delta}$ as the order parameter determined numerically from $\ln(\hat{\Delta}(\alpha)/\Delta_0) = -\pi\alpha/4\hat{\Delta}(\alpha)$ for a given pair breaking parameter α.[46,47] The latter we interpolate as $\alpha = 0.5\Delta_0^*(B/B_c)^n$ with n a characteristic exponent. As shown in Figure 2e, the best fit we obtain for n = 3, Δ_0^* = 1.12 meV and the (upper) critical field B_c = 14.5 T. The latter value is clearly larger than reported for bulk MoRe. Seemingly similar data plotted as purple stars and blue rectangles are discussed below.

As expected for a superconducting energy gap, Δ* is also reduced with increasing temperature T. In Figure 2f, we plot G_{23} (contact distance of ∼1.55 μm) as a function of V_{SD} at V_{BG} = 9 V for a series of temperatures at B = 0 in a different cooldown. For the lowest values of T, we can reproduce the data using very similar BTK and Dynes parameters as above, only adjusting the normal state resistance and the temperature to T = 1.7 K. However, at higher temperatures, the fits become ambiguous, due to a broadening and possibly a temperature dependence of the Schottky barrier.[30] Again, we plot the inflection points of the curves as an estimate for Δ*, as shown in Figure 2g. To determine the critical temperature, we fit the expression $\Delta^* = \Delta_0^*\sqrt{1 - T/T_c}$ and find T_c = 7.7 K and Δ_0^* = 1.2 meV, consistent with literature values for bulk MoRe.[38,39]

Up to this point, our experiments demonstrate superconducting contacts but with a weak electronic coupling between the MoS_2 and the reservoirs, at least for one contact interface. However, we also find evidence for a stronger coupling of MoS_2 regions to the superconductors, relevant for devices relying on the superconducting proximity effect. As an example, we show bias spectroscopy measurements with CB features between contacts C_1 and C_2 (distance ∼2.5 μm) in Figure 3 for a series of magnetic fields B. Similarly as in Figure 2, we find a transport gap, reduced by larger B values. Here, the

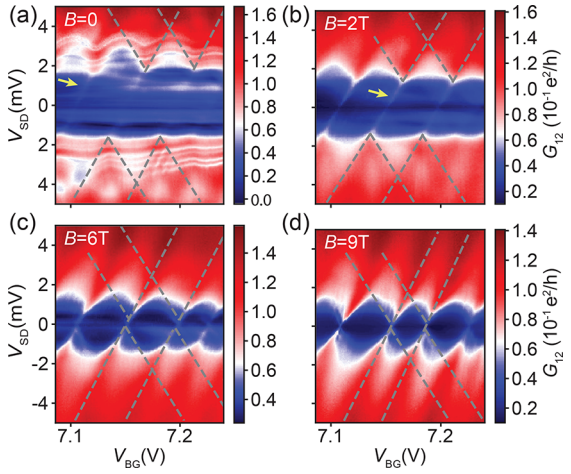

Figure 3. G_{12} plotted as a function of V_{BG} and V_{SD} at (a) B = 0, (b) B = 2 T, (c) B = 6 T, and (d) B = 9 T, recorded at T = 60 mK. The dashed lines trace the CB diamonds, shifted vertically and horizontally between the subfigures, while the yellow arrows point out lines of resonant Andreev tunneling.

https://doi.org/10.1021/acs.nanolett.1c00615
Nano Lett. 2021, 21, 5614−5619

low-bias ends of the CB diamonds are shifted in energy and in gate voltage, as indicated by the gray dashed lines, consistent with a MoS_2 quantum dot (QD) directly coupled to one superconducting contact (i.e., forming an S-QD-N junction).[48] These tips of the CB diamonds are connected across the gap by a single faint resonance, pointed out by yellow arrows, best seen in Figure 3b at B = 2 T. We attribute these lines to resonant Andreev tunneling,[48] in which the electrons of a Cooper pair pass through the QD in a higher order tunneling process. This process is suppressed much stronger by a tunnel barrier than single particle tunneling,[49] which suggests that the QD is strongly coupled to the superconductor. At large B fields, a quasi-particle background in the superconducting density of states results in single particle CB diamonds.[42] With a QD charging energy of ∼2 meV and using $E_c = \frac{e^2}{8\epsilon\epsilon_0 r}$ for a disc shaped QD encapsulated in hBN, we estimate the radius of the confined QD region as $r \approx 300$ nm.

The shift of the CB diamonds in V_{SD} gives a measure for Δ^*,[48] which we read out at the bias at which ∼50% of the large bias conductance is reached at the tip of the CB diamond. The extracted values are plotted as purple stars in Figure 2e. Surprisingly, we find a significantly larger zero field gap, $\Delta_0^* \approx$ 1.7 meV, and a rather different functional dependence on B than for the curves analyzed in Figure 2 (red dots). The latter is demonstrated by the dotted line obtained for the exponent n = 2, and B_c = 6.4 T. In addition, Figure 2e shows a third Δ^* curve extracted from CB diamond shifts in experiments on another contact pair shown in Supporting Information, Figure S2. For this curve, we obtain n = 1, while $\Delta^* \approx$ 1.12 meV and $B_c \approx$ 12 T correspond well to the previously obtained values.

While a larger gap in the transport experiments can be simply attributed to a significant fraction of the bias developing across another part of the device, for example, across the second N/S junction, the different functional dependence is more difficult to explain. Since nominally the geometry and MoRe film thickness are identical for all contacts, we tentatively attribute this finding to a superconducting proximity region forming in the MoS_2 near a strongly couped contact, yielding an induced superconducting energy gap Δ^*,[42] and a different B-field dependence of the pair breaking compared to the bulk superconductor.

Additional indications for a stronger coupling to S are the almost gate voltage independent features at B = 0, reminiscent of two NS junctions and multiple Andreev reflection processes in between, with a much stronger suppression with increasing B than for the observed gap. In Supporting Information, Figure S3a, we also show data at higher gate voltages, exhibiting a conductance minimum instead of a maximum at the bias that corresponds to the energy gap, developing into negative differential conductance at the lowest field values. These findings are qualitatively consistent with calculations for an S/I/N/S junction with resonances in the N region.[50]

The above data show that our fabrication scheme results in superconducting contacts to monolayer MoS_2, possibly with a reasonably strong coupling to the superconductors for some of the contacts. To demonstrate that the intrinsic properties of MoS_2 are intact in the bulk crystal, we investigate quantum transport in large magnetic fields and at bias voltages large enough to render the superconducting energy gap irrelevant. In Figure 4a, we plot the dc conductance $G_{12} = I_1/V_{SD}$ as a function of V_{BG} and B, at V_{SD} = 8 mV and T = 60 mK, from which we have subtracted a third order polynomial background

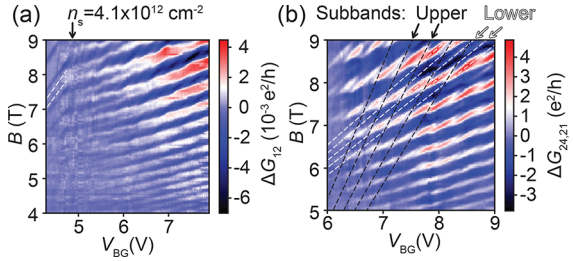

Figure 4. (a) Two-terminal dc conductance $G_{12} = I_1/V_{SD}$ with V_{SD} = 8 mV applied to contact C_2, plotted as a function of the magnetic field B and the backgate voltage V_{BG} at $T \approx$ 60 mK. n_s points out the gate voltage corresponding to the electron density at which the higher spin−orbit subbands start to be populated. (b) Three-terminal dc conductance $G_{24,21} = I_2/V_{12}$ with an external bias V_{SD} = 10 mV applied to C_4, while the current I_2 is measured at C_2 and the voltage difference V_{12} between C_1 and C_2. In both maps, a third order polynomial was subtracted at each gate voltage to remove a smooth background.

for each gate voltage to eliminate effects from the classical Hall effect and CB effects.

Figure 4a shows well developed Shubnikov de Haas (SdH) oscillations, suggesting a high MoS_2 quality, with an onset at B_{on} < 4 T. In the Drude model, this onset is interpreted as the charge carriers closing a cyclotron orbit before being scatted, which happens roughly at $\omega_c\tau > 1$, with $\omega_c = eB/m^*$ the cyclotron frequency, m^* the effective electron mass, and τ the scattering time. This yields a lower bound for the carrier mobility of $\mu = e\tau/m^* \approx 2500$ cm^2/(Vs), similar to $\mu \approx 5000$ cm^2/(Vs) that we obtain with Au VIA contacts, identical to the best literature values.[24] The discrepancy in mobility between the MoRe and the Au VIA contacts we attribute to heating effects due to the much larger bias we apply to the MoRe contacts to avoid effects of the superconducting energy gap.

The quality of the MoS_2 can also be seen in the fact that the four lowest spin−orbit subbands, corresponding to the valley and the spin degree of freedom, are not mixed by disorder. We find that the slope of the SdH resonances changes by roughly a factor of 2 at V_{BG} = 4.8 V, corresponding to an electron density of $n_s \approx 4.1 \times 10^{12}$ cm^{-2} at which the two upper spin−orbit subbands become populated. Using m^* = 0.6, we obtain a subband spacing of ∼15 meV, as reported previously.[23] These features prevail also at $T \approx$ 1.7 K, as shown in Supporting Information, Figure S3b.

The two-terminal magneto-conductance measurements suffer from large background resistances due to Schottky barriers, which we can partially circumnavigate by performing a three terminal experiment. In Figure 4b, we plot the dc conductance $G_{24,21}$, as explained in the figure caption. This technique removes the contact resistance at C4 so that the conductance resonances due to the Landau levels can be measured more clearly. The results in Figure 4b show similar patterns as in better suited Hall bar experiments,[23] exhibiting clear superposition patterns of the spin and valley split subbands, indicated by dashed lines. We note that due to the less ideal contact geometry of our devices, we cannot go to lower electron densities in these experiments, because the current density passing near the remote contacts is very low.

In conclusion, we established superconducting contacts to a monolayer of the TMDC semiconductor MoS_2 using vertical interconnect access (VIA) contacts and characterized the superconducting energy gap in different transport regimes. In most experiments, one N/S junction dominates the transport

https://doi.org/10.1021/acs.nanolett.1c00615
Nano Lett. 2021, 21, 5614−5619

characteristics, as well as signatures of resonant Andreev tunneling and a superconducting proximity effect, suggesting that contacts with a stronger transmission between the superconductor and the semiconductor are also possible, thus opening a path toward semiconductor−superconductor hybrid devices at the limit of miniaturization with a group of materials, the TMDCs, that offers a very large variety of material properties and physical phenomena.

■ ASSOCIATED CONTENT

Supporting Information

The Supporting Information is available free of charge at https://pubs.acs.org/doi/10.1021/acs.nanolett.1c00615.

Additional data Figures S1, S2, and S3; gate and magnetic field dependence obtained on a second device, Coulomb blockade diamond analysis obtained for a second contact pair (C_2 and C_3), bias spectroscopy data for G_{12} at the larger backgate voltage V_{BG} = 9.0 V, and Shubnikov de Haas oscillations (Landau fan) at a temperature of ∼1.7 K (PDF)

■ AUTHOR INFORMATION

Corresponding Author

Andreas Baumgartner − *Department of Physics, University of Basel, CH-4056 Basel, Switzerland; Swiss Nanoscience Institute, University of Basel, CH-4056 Basel, Switzerland;* orcid.org/0000-0003-4681-4926; Email: andreas.baumgartner@unibas.ch

Authors

Mehdi Ramezani − *Department of Physics, University of Basel, CH-4056 Basel, Switzerland; Swiss Nanoscience Institute, University of Basel, CH-4056 Basel, Switzerland*

Ian Correa Sampaio − *Department of Physics, University of Basel, CH-4056 Basel, Switzerland;* orcid.org/0000-0002-4150-1886

Kenji Watanabe − *Research Center for Functional Materials, National Institute for Material Science, Tsukuba 305-0044, Japan;* orcid.org/0000-0003-3701-8119

Takashi Taniguchi − *International Center for Materials Nanoarchitectonics, National Institute for Materials Science, Tsukuba 305-0044, Japan;* orcid.org/0000-0002-1467-3105

Christian Schönenberger − *Department of Physics, University of Basel, CH-4056 Basel, Switzerland; Swiss Nanoscience Institute, University of Basel, CH-4056 Basel, Switzerland;* orcid.org/0000-0002-5652-460X

Complete contact information is available at: https://pubs.acs.org/10.1021/acs.nanolett.1c00615

Notes

The authors declare no competing financial interest.

All data sets in this publication are available in numerical form at https://doi.org/10.5281/zenodo.4899933.

■ ACKNOWLEDGMENTS

This work was supported financially by the Swiss National Science Foundation project "Two-dimensional semiconductors for superconductor hybrid nanostructures" granted to A.B., the Swiss Nanoscience Institute (SNI) project P1701, and the ERC project Top-Supra (787414). K.W. and T.T. acknowledge support from the Elemental Strategy Initiative conducted by the MEXT, Japan, Grant JPMXP0112101001, JSPS KAKENHI Grant JP20H00354, and the CREST (JPMJCR15F3), JST.

■ REFERENCES

(1) Larsen, T. W.; Petersson, K. D.; Kuemmeth, F.; Jespersen, T. S.; Krogstrup, P.; Nygård, J.; Marcus, C. M. Semiconductor-nanowire-based superconducting qubit. *Phys. Rev. Lett.* **2015**, *115*, 127001.

(2) Leivo, M.; Pekola, J.; Averin, D. Efficient Peltier refrigeration by a pair of normal metal/insulator/superconductor junctions. *Appl. Phys. Lett.* **1996**, *68*, 1996.

(3) Roddaro, S.; Pescaglini, A.; Ercolani, D.; Sorba, L.; Giazotto, F.; Beltram, F. Hot-electron effects in InAs nanowire Josephson junctions. *Nano Res.* **2011**, *4*, 259.

(4) Mourik, V.; Zuo, K.; Frolov, S. M.; Plissard, S.; Bakkers, E. P.; Kouwenhoven, L. P. Signatures of Majorana fermions in hybrid superconductor-semiconductor nanowire devices. *Science* **2012**, *336*, 1003.

(5) Deng, M.; Vaitiekėnas, S.; Hansen, E. B.; Danon, J.; Leijnse, M.; Flensberg, K.; Nygård, J.; Krogstrup, P.; Marcus, C. M. Majorana bound state in a coupled quantum-dot hybrid-nanowire system. *Science* **2016**, *354*, 1557.

(6) Hofstetter, L.; Csonka, S.; Nygård, J.; Schönenberger, C. Cooper pair splitter realized in a two-quantum-dot Y-junction. *Nature* **2009**, *461*, 960.

(7) Hofstetter, L.; Csonka, S.; Baumgartner, A.; Fülöp, G.; d'Hollosy, S.; Nygård, J.; Schönenberger, C. Finite-bias Cooper pair splitting. *Phys. Rev. Lett.* **2011**, *107*, 136801.

(8) Fülöp, G.; d'Hollosy, S.; Baumgartner, A.; Makk, P.; Guzenko, V.; Madsen, M.; Nygård, J.; Schönenberger, C.; Csonka, S. Local electrical tuning of the nonlocal signals in a Cooper pair splitter. *Phys. Rev. B: Condens. Matter Mater. Phys.* **2014**, *90*, 235412.

(9) Wan, Z.; Kazakov, A.; Manfra, M. J.; Pfeiffer, L. N.; West, K. W.; Rokhinson, L. P. Induced superconductivity in high-mobility two-dimensional electron gas in gallium arsenide heterostructures. *Nat. Commun.* **2015**, *6*, 7426.

(10) Casparis, L.; Connolly, M. R.; Kjaergaard, M.; Pearson, N. J.; Kringhøj, A.; Larsen, T. W.; Kuemmeth, F.; Wang, T.; Thomas, C.; Gronin, S.; et al. Superconducting gatemon qubit based on a proximitized two-dimensional electron gas. *Nat. Nanotechnol.* **2018**, *13*, 915.

(11) Fornieri, A.; Whiticar, A. M.; Setiawan, F.; Portolés, E.; Drachmann, A. C.; Keselman, A.; Gronin, S.; Thomas, C.; Wang, T.; Kallaher, R.; et al. Evidence of topological superconductivity in planar Josephson junctions. *Nature* **2019**, *569*, 89.

(12) Vischi, F.; Carrega, M.; Braggio, A.; Paolucci, F.; Bianco, F.; Roddaro, S.; Giazotto, F. Electron Cooling with Graphene-Insulator-Superconductor Tunnel Junctions for Applications in Fast Bolometry. *Phys. Rev. Appl.* **2020**, *13*, 054006.

(13) Graziano, G. V.; Lee, J. S.; Pendharkar, M.; Palmstrøm, C. J.; Pribiag, V. S. Transport studies in a gate-tunable three-terminal Josephson junction. *Phys. Rev. B: Condens. Matter Mater. Phys.* **2020**, *101*, 054510.

(14) Xiao, D.; Liu, G.-B.; Feng, W.; Xu, X.; Yao, W. Coupled spin and valley physics in monolayers of MoS 2 and other group-VI dichalcogenides. *Phys. Rev. Lett.* **2012**, *108*, 196802.

(15) Bhowal, S.; Satpathy, S. Intrinsic orbital and spin Hall effects in monolayer transition metal dichalcogenides. *Phys. Rev. B: Condens. Matter Mater. Phys.* **2020**, *102*, 035409.

(16) Žutić, I.; Fabian, J.; Sarma, S. D. Spintronics: Fundamentals and applications. *Rev. Mod. Phys.* **2004**, *76*, 323.

(17) Wang, Q. H.; Kalantar-Zadeh, K.; Kis, A.; Coleman, J. N.; Strano, M. S. Electronics and optoelectronics of two-dimensional transition metal dichalcogenides. *Nat. Nanotechnol.* **2012**, *7*, 699.

(18) Kormányos, A.; Zólyomi, V.; Drummond, N. D.; Burkard, G. Spin-orbit coupling, quantum dots, and qubits in monolayer transition metal dichalcogenides. *Phys. Rev. X* **2014**, *4*, 011034.

(19) Qiu, D. Y.; da Jornada, F. H.; Louie, S. G. Optical spectrum of MoS 2: many-body effects and diversity of exciton states. *Phys. Rev. Lett.* **2013**, *111*, 216805.
(20) Kormányos, A.; Burkard, G.; Gmitra, M.; Fabian, J.; Zólyomi, V.; Drummond, N. D.; Fal'ko, V. k· p theory for two-dimensional transition metal dichalcogenide semiconductors. *2D Mater.* **2015**, *2*, 022001.
(21) Tang, S.; Zhang, C.; Wong, D.; Pedramrazi, Z.; Tsai, H.-Z.; Jia, C.; Moritz, B.; Claassen, M.; Ryu, H.; Kahn, S.; et al. Quantum spin Hall state in monolayer 1T'-WTe 2. *Nat. Phys.* **2017**, *13*, 683.
(22) Miserev, D.; Klinovaja, J.; Loss, D. Exchange intervalley scattering and magnetic phase diagram of transition metal dichalcogenide monolayers. *Phys. Rev. B: Condens. Matter Mater. Phys.* **2019**, *100*, 014428.
(23) Pisoni, R.; Kormányos, A.; Brooks, M.; Lei, Z.; Back, P.; Eich, M.; Overweg, H.; Lee, Y.; Rickhaus, P.; Watanabe, K.; et al. Interactions and magnetotransport through spin-valley coupled Landau levels in monolayer MoS 2. *Phys. Rev. Lett.* **2018**, *121*, 247701.
(24) Pisoni, R.; Lei, Z.; Back, P.; Eich, M.; Overweg, H.; Lee, Y.; Watanabe, K.; Taniguchi, T.; Ihn, T.; Ensslin, K. Gate-tunable quantum dot in a high quality single layer MoS2 van der Waals heterostructure. *Appl. Phys. Lett.* **2018**, *112*, 123101.
(25) Marega, G. M.; Zhao, Y.; Avsar, A.; Wang, Z.; Tripathi, M.; Radenovic, A.; Kis, A. Logic-in-memory based on an atomically thin semiconductor. *Nature* **2020**, *587*, 72−77.
(26) Island, J. O.; Steele, G. A.; van der Zant, H. S.; Castellanos-Gomez, A. Thickness dependent interlayer transport in vertical MoS2 Josephson junctions. *2D Mater.* **2016**, *3*, 031002.
(27) Trainer, D. J.; Wang, B.; Bobba, F.; Samuelson, N.; Xi, X.; Zasadzinski, J.; Nieminen, J.; Bansil, A.; Iavarone, M. Proximity-Induced Superconductivity in Monolayer MoS2. *ACS Nano* **2020**, *14*, 2718.
(28) Costanzo, D.; Jo, S.; Berger, H.; Morpurgo, A. F. Gate-induced superconductivity in atomically thin MoS 2 crystals. *Nat. Nanotechnol.* **2016**, *11*, 339.
(29) Roch, J. G.; Froehlicher, G.; Leisgang, N.; Makk, P.; Watanabe, K.; Taniguchi, T.; Warburton, R. J. Spin-polarized electrons in monolayer MoS 2. *Nat. Nanotechnol.* **2019**, *14*, 432.
(30) Cui, X.; Lee, G.-H.; Kim, Y. D.; Arefe, G.; Huang, P. Y.; Lee, C.-H.; Chenet, D. A.; Zhang, X.; Wang, L.; Ye, F.; et al. Multi-terminal transport measurements of MoS 2 using a van der Waals heterostructure device platform. *Nat. Nanotechnol.* **2015**, *10*, 534.
(31) Allain, A.; Kang, J.; Banerjee, K.; Kis, A. Electrical contacts to two-dimensional semiconductors. *Nat. Mater.* **2015**, *14*, 1195−1205.
(32) Schauble, K.; Zakhidov, D.; Yalon, E.; Deshmukh, S.; Grady, R. W.; Cooley, K. A.; McClellan, C. J.; Vaziri, S.; Passarello, D.; Mohney, S. E.; Toney, M. F.; Sood, A.; Salleo, A.; Pop, E. Uncovering the Effects of Metal Contacts on Monolayer MoS2. *ACS Nano* **2020**, *14*, 14798−14808.
(33) Samm, J.; Gramich, J.; Baumgartner, A.; Weiss, M.; Schönenberger, C. Optimized fabrication and characterization of carbon nanotube spin valves. *J. Appl. Phys.* **2014**, *115*, 174309.
(34) Lembke, D.; Bertolazzi, S.; Kis, A. Single-layer MoS2 electronics. *Acc. Chem. Res.* **2015**, *48*, 100.
(35) Seredinski, A.; Arnault, E.; Costa, V.; Zhao, L.; Larson, T.; Watanabe, K.; Taniguchi, T.; Amet, F.; Newaz, A.; Finkelstein, G. One-Dimensional Edge Contact to Encapsulated MoS2 with a Superconductor. *AIP Adv.* **2021**, *11*, 045312.
(36) Telford, E. J.; Benyamini, A.; Rhodes, D.; Wang, D.; Jung, Y.; Zangiabadi, A.; Watanabe, K.; Taniguchi, T.; Jia, S.; Barmak, K.; et al. Via method for lithography free contact and preservation of 2D Mater. *Nano Lett.* **2018**, *18*, 1416.
(37) Witcomb, M.; Dew-Hughes, D. The σ-phase in molybdenum-rhenium; microstructure and superconducting hysteresis. *J. Less-Common Met.* **1973**, *31*, 197.
(38) Sundar, S.; Sharath Chandra, L.; Sharma, V.; Chattopadhyay, M.; Roy, S. Electrical transport and magnetic properties of superconducting Mo 52 Re 48 alloy. *AIP Conf. Proc.* **2012**, 1092−1093.
(39) Singh, V.; Schneider, B. H.; Bosman, S. J.; Merkx, E. P.; Steele, G. A. Molybdenum-rhenium alloy based high-Q superconducting microwave resonators. *Appl. Phys. Lett.* **2014**, *105*, 222601.
(40) Pillet, J-D.; Quay, C. H. L.; Morfin, P.; Bena, C.; Yeyati, A. L.; Joyez, P. Andreev bound states in supercurrent-carrying carbon nanotubes revealed. *Nat. Phys.* **2010**, *6*, 965.
(41) Gramich, J.; Baumgartner, A.; Schönenberger, C. Andreev bound states probed in three-terminal quantum dots. *Phys. Rev. B: Condens. Matter Mater. Phys.* **2017**, *96*, 195418.
(42) Jünger, C.; Baumgartner, A.; Delagrange, R.; Chevallier, D.; Lehmann, S.; Nilsson, M.; Dick, K. A.; Thelander, C.; Schönenberger, C. Spectroscopy of the superconducting proximity effect in nanowires using integrated quantum dots. *Commun. Phys.* **2019**, *2*, 1.
(43) Heedt, S.; Quintero-Pérez, M.; Borsoi, F.; Fursina, A.; van Loo, N.; Mazur, G. P.; Nowak, M. P.; Ammerlaan, M.; Li, K.; Korneychuk, S., et al. Shadow-wall lithography of ballistic superconductor-semiconductor quantum devices. arXiv preprint arXiv:2007.14383 **2020**.
(44) Blonder, G.; Tinkham, M.; Klapwijk, T. Transition from metallic to tunneling regimes in superconducting microconstrictions: Excess current, charge imbalance, and supercurrent conversion. *Phys. Rev. B: Condens. Matter Mater. Phys.* **1982**, *25*, 4515.
(45) Dynes, R.; Narayanamurti, V.; Garno, J. P. Direct measurement of quasiparticle-lifetime broadening in a strong-coupled superconductor. *Phys. Rev. Lett.* **1978**, *41*, 1509.
(46) Skalski, S.; Betbeder-Matibet, O.; Weiss, P. Properties of Superconducting Alloys Containing Paramagnetic Impurities. *Phys. Rev.* **1964**, *136*, A1500.
(47) Gramich, J.; Baumgartner, A.; Schönenberger, C. Subgap resonant quasiparticle transport in normal-superconductor quantum dot devices. *Appl. Phys. Lett.* **2016**, *108*, 172604.
(48) Gramich, J.; Baumgartner, A.; Schönenberger, C. Resonant and inelastic Andreev tunneling observed on a carbon nanotube quantum dot. *Phys. Rev. Lett.* **2015**, *115*, 216801.
(49) Sun, Q.-f.; Wang, J.; Lin, T.-h. Resonant Andreev reflection in a normal-metal−quantum-dot−superconductor system. *Phys. Rev. B: Condens. Matter Mater. Phys.* **1999**, *59*, 3831.
(50) Zhitlukhina, E.; Devyatov, I.; Egorov, O.; Belogolovskii, M.; Seidel, P. Anomalous inner-gap structure in transport characteristics of superconducting junctions with degraded interfaces. *Nanoscale Res. Lett.* **2016**, *11*, 1.

https://doi.org/10.1021/acs.nanolett.1c00615
Nano Lett. 2021, 21, 5614−5619